Research Square

Preprints are preliminary reports that have not undergone peer review.
They should not be considered conclusive, used to inform clinical practice,
or referenced by the media as validated information.

Subglacial landscape reveal potential future glacial lakes in the Southern Andes

Jorge Berkhoff

jorge.andres.berkhoff@fau.de

Friedrich-Alexander-Universität Erlangen-Nürnberg

David Farias

Universidad de Concepción https://orcid.org/0009-0002-2385-7923

Pablo Iribarren-Anacona

Austral University of Chile

Christian Sommer

University of Erlangen-Nuremberg https://orcid.org/0000-0002-6641-0681

José Uribe

Instituto de Ciencia y Exploración (ice)

Johannes Fürst

Friedrich-Alexander-Universität Erlangen-Nürnberg https://orcid.org/0000-0003-3988-5849

Article

Keywords:

Posted Date: August 25th, 2026

DOI: https://doi.org/10.21203/rs.3.rs-10743366/v1

License: This work is licensed under a Creative Commons Attribution 4.0 International License.
Read Full License

Additional Declarations: There is **NO** Competing Interest.

Subglacial landscape reveal potential future glacial lakes in the Southern Andes

Jorge Berkhoff[1], David Farías-Barahona[2], Pablo Iribarren-Anacona[3], Christian Sommer[1], Marius Schaefer[4], José Luis Rodríguez[4], José Uribe[5], Johannes J. Fürst[1].

Affiliation

[1]Department of Geography, Friedrich-Alexander-Universität Erlangen-Nürnberg, Erlangen, Germany

[2]Department of Geography, University of Concepcíon, Concepción, Chile

[3] Institute of Earth Sciences, Austral University of Chile, Valdivia, Chile

[4]Institute of Physical and Mathematical Sciences, Austral University of Chile, Valdivia, Chile

[5] Instituto de Ciencia y Exploración, (ice) Valdivia, Chile

Abstract

As mountain glaciers retreat depression/over-deepening in the now bare topography can retain some of the meltwater previously stored as glacier ice. Yet the location and volume of these future glacial lakes have never been mapped for an entire glacierised region. Here we present the first regional reconstruction of ice thickness and subglacial topography for the Southern Andes, calibrated with ground-penetrating radar and updated RGI7 outlines. We find a total glacier volume of 5961 ± 1981 km^3, a sea-level equivalent of 14.8 ± 4.99 mm, of which the three Patagonian Icefields hold more than 97%. Removing this ice from the terrain reveals 3951 overdeepenings capable of becoming lakes, storing a potential of 298.6 ± 11.0 km^3 of water: about 5% of the region's ice, an unusually high interception fraction that exceeds every other mountain range where the exercise has been repeated. The spatial distribution of future lake volumes is far from uniform. While less than 1% of all sites, mostly in Patagonia, hold half of the total lake

volume, the Dry and Central Andes – where glaciers currently assure/play a crucial role for seasonal freshwater security - only accommodate for less than 2%, By resolving where deglaciation will store water, and by withholding of order 4% of the regions ice from the ocean, these maps provide a physical basis for anticipating both the water resources and the outburst flood hazards that will accompany the end of the Andean glaciation

Introduction

Climate change has intensified ice loss in glacierised mountain ranges worldwide, driving transformations in hydrological, geomorphological, and environmental systems (Xu et al., 2009). As glaciers retreat and the underlying topography becomes ice-free, overdeepenings now covered will fill with water, and the population of lakes in mountain regions will continuously grow in the future (Carrivick et al., 2013; Shugar et al., 2020; Frank et al., 2026). These changes not only affect mountain ecosystems but also threaten local communities As mountain glaciers retreat entails increasing risk from slope instabilities and glacial lake outbursts (GLOFs), i.e. natural hazards in mountain region (Iribarren-Anacona et al., 2014; Carrivick et al., 2016). In this context, it is vital to understand glacier evolution in this high-relief topography to anticipate natural hazards, invest in sustainable water resources management, and mitigate social and environmental impacts in mountainous regions (Furian et al., 2021).

The Andean cordillera is the main mountain range in South America. It harbour thousands of glaciers cross their entire latitudinal extent – from Venezuela in the north to Chile in the south. This cordillera represents one of the most important water towers around the world, making it vital for downstream freshwater security (Immerzeel et al., 2020). According to the Randolph Glacier

Inventory (RGI) (RGI7.0 Consortium, 2023), the system is divided into the Tropical Andes and the Southern Andes, the latter extending from ~23°S to 56°S.), the system is divided into the Tropical Andes and the Southern Andes, the latter extending from ~23°S to 56°S. This Southern sector contains a striking diversity of glacier types, from high-elevation rock glaciers in the north to the largest temperate ice masses in the Southern Hemisphere outside Antarctica in the south. Following the regional classification of Masiokas et al. (2009) and Sagredo and Loweel (2012), the Southern Andes can be divided into four glaciological regions defined by distinct climatic and topographic conditions: the Dry Andes, the Central Andes, the Northern Patagonian Andes (Lake District), and the Southern Patagonian Andes.

These regions span a strong north to south gradient in both glacier geometry and climat, from small, hifh elevation, topographically controlled mountain glaciers in the arid north to the vast, low reaching icefields of humid Patagonia in the south. In the Dry Andes and Central Andes, glaciers are small and located at high elevations, i.e. the classic topographically controlled mountain glacier type. Their abundance decreases markedly the further we look to the north (Caro et al., 2021) As we move northward, climatic conditions turn increasingly arid, and the little precipitation is insufficient to sustain a large glacier population — where glaciers persist at all, they do so only at selected, sheltered sites (Caro et al., 2021; Dussaillant et al., 2019; Minowa et al., 2021). Further south in the Northern and Southern Patagonian Andes, the setting shifts to vast icefields showing a multitude of elongated outlet glacier that extend to low elevations. In the west many of them reach the Pacific Ocean. In the east they often terminate in proglacial lakes. In the south, we encounter three of the largest ice bodies of the Southern Hemisphere, i.e. the Northern Patagonian Icefield (NPI), the Southern Patagonian Icefield (SPI), and the Cordillera Darwin Icefield (CDI), together covergin ~15,700 km^2, and this region shows one of the highest rates of

glaciers mass loss anywhere on Earth, with ~83% of the continents glacier mass loss occurring in the Patagonian icefields (Braun et al., 2019; Hugonnet et al., 2021; The GlaMBIE Team, 2025). These Icefields combine high mass overturning with the extraordinary speeds of their outlet glaciers and some of the highest basal-erosion rates measured worldwide, contemporary erosion rates across 15 outlet glaciers between Patagonia and the Atartic Peninsula span three orders of magnitude and scale with climate, with the Patagonian Icefields sitting at the erosive end of that transect (Koppes et al., 2015). This is why we expect a particularly large potential for future glacial lakes in Patagonia.

Although the Dry Andes and Central Andes hold only a small fraction of the region ice, that ice lies upstream of the country most densely populated, arid and semi arid basins, where it is a strategic element of year round freshwater security. This is most evident in the Cnetral Andes, the Snatiago Metropolitan area, home to nearly seven million people, draws a large part of its supply from the Maipo river basin, which hass benn under megradrought since 2010, the driest sustained period in the instrumental record and unprecedent in recents centuries (Garreaud et al., 2020). Through that drought, glacier melt has buffered the late-summer discharge of the Maipo, between 2010 and 2018 the imbalance component of glacier ablation supplied a water equivalent volume of 740×10^6 m^3, about 3.4 times the capacity of the El Yeso reservoir and equivalent to 14% of Santiago potable water use (McCarthy et al., 2022). This buffering, however draws on net mass loss and cannot persist, peak water for the subtropical Andes is thought have already passed (Huss and Hock, 2018), and the regions glaciers are projected to lose a large part of their present volume by 2100.

As current glacier retreat is momentous, reliable knowledge of ice thickness and subglacial topography are essential. Yet direct observation only exist for a negligible fraction of all glaciers

(GlaThiDa). We therefore rely on reconstruction models using surface quantities to best infer maps of the landscape beneath the current ice cover. These not only serve to estimate the available ice volume (Fürst et al., 2018; Farinotti et al., 2019), but they also help to localize topographic overdeepening that may accommodate lakes once the glacier ice retreated (Linsbauer et al., 2012; Frey et al., 2014; Furian et al., 2021). Identification and reliable characterization of such lakes is not only critical for GLOF hazard assessment, but also with regard to phases overall glacier retreat as such settings allow for speed-up and self-accelerating retreat of marine and lake-terminating (MALT) ice fronts. Such phases of facilitated retreat is well documented for the SPI (e.g., Upsala, Jorge Montt) and the CDI (Marinelli). Even a limited number of lakes can substantially modify drainage networks and elevte GLOF hazard (Carrivick and Tweed, 2013; Wilson et al., 2018) at least 16 moraine-dammed lakes have failed in Patagonia in historical time, and Patagonian outburst flood have destroyed houses, forced the relocation of a village caused three deaths (Iribarren-Anacona et al., 2015).In the first years after formation, these lakes are especially prone to GLOF generation (Emmer et al., 2017).

In recent decades, models have been developed to estimate ice thickness at regional and global scales (Huss and Farinotti, 2012; Maussion et al., 2019; Millan et al., 2022; Frank et al., 2026). These estimates have been essential for improving our knowledge of present glacier ice volume and for projecting their future behaviour. Many of the existing models have participate in a collaborative effort to produce a ‘consensus estimate’ of ice thickness for all glaciers on Earth (Farinotti et al., 2017). This endeavour highlights the importance of local to regional calibration. In the Southern Andes, however, all existing map products suffer from little or no direct thickness observations. As a consequen, these estimates do not necessarily agree well amongst each other or with repsect to available GPR measurements. This underscores the need for a regionally calibrated

reconstruction accounting for the existing wealth of ground-truth thickness measurements. Reconstrcting glacier ice thickness in the Southern Andes poses significant challenges due to limited direct measurements, such as Ground Penetrating Radar (GPR) data, and the absence of comprehensive surface mass-balance models. In this study, we substantially expand the observational basis four our ice thickness model reconstruction in the Southern Andes to 48 gkacuers that had no previously been used in any region or global products. Moreover, we incorporate glacier retreat information which constrains pasth ice thickness cloase to the current glacier retreat fronts (Sommer et al., 2023). Together with the update RGI7 glacier outlines, this approach, combining an expanded GPR record (Koch et al., 2025; Koch et al., 2026) with geodetic mass balance to inger past ice thickness, allows us to regionally calibrate an ice thickness model (Fürst et al., 2018; Fürst et al., 2024).) based on the critical basal shear stress, assuming perfect plasticity. (Frey et al., 2014)

Applying this perfect-plasticity method, we produce thickness maps reference to the year 2000 (SRTM) for the updated RGI7 outlines, covering all Chilean and Argentinean glaciers across the Southern Andes (23°S to 56°S). Based on this information a model of the subglacial topographt has been created for the current glaciers in the Southern Andes, which serves as the baseline for identifying potential sites of future glacial lakes formation. This model identifies topographic depessions that are likely to fill with water in the future, contributing to the first inventory of potential zones for the formation of future glacial lakes.

Results

Mapping ice thickness in the Southern Andes

Across the Southern Andes, we estimate a total glacier volume of 5,960 ± 1,980 km^3 (Table 1). This ice thickness is distributed very unevenly across the region's four climatological zones. The Southern Patagonian Andes hold the overwhelming majority of the ice, with a total volume of 5.808 km^3 and the highest mean ice thickness of all regions (247 meters), whereas the three remaining zones together account for less than 3% of the total volume.

Also in the Southern Patagonian Andes, almost 95% (54,83) of the glacier ice is stored in only three icefields i.e NPI, SPI y CDI, across a combined area of 18,352 km^2. The 16,6719 outside these icefields stored a remaining 5.6% (325). These show more northern regions only stored 1.1%, 1.3% and 0.1% the total ice volume, respectively for the Northern Patagonia, Central Andes and Dry Ande. Mean values of ice thickness follows a similar pattern amounting to 38.1 m, 53.4 m and 31.3 m, respectively. Associated uncertainties fall into the range of 30-40% (Table 1). These relative values are not negligible and reflect the generally scarce availability of in-situ measurements.

Transforming these reginoal volumes into a sea-level equivalent (SLE, Table 1), we account for the ice that will not reach the ocean. We first apply a flotation correction to the marine-terminating glaciers (62 glaciers calssified as tidewater in RGI7, all located in Southern Patagonian Andes), counting only the ice above flotation by removing the columm grounded below sea level that would otherwise displace ocean water. In addition, part of the released water will later be stored on land in future glacial lakes rather than reaching the ocean, expressed in ice equivalent, this amounts to about 5% of total ice volume, of which fraction above sea level is genuinely withheld from the ocean. Acoounting for both effects, thse Southern Andes represent a total potential sea-level contribution of 14.5 ± 4.9 mm.

Fig. 1: Latitudinal distribution, mean ice thickness, and cumulative ice volume in the Southern Andes. (a) Mean ice thickness and the glacierized area in each cell, with an inset showing the latitudinal distribution of mean ice thickness (red) and glacierized area (grey) (b) total ice volume per cell. (c) Glaciers coloured by glaciological region following the latitudinal profile of Masiokas et al. (2009).

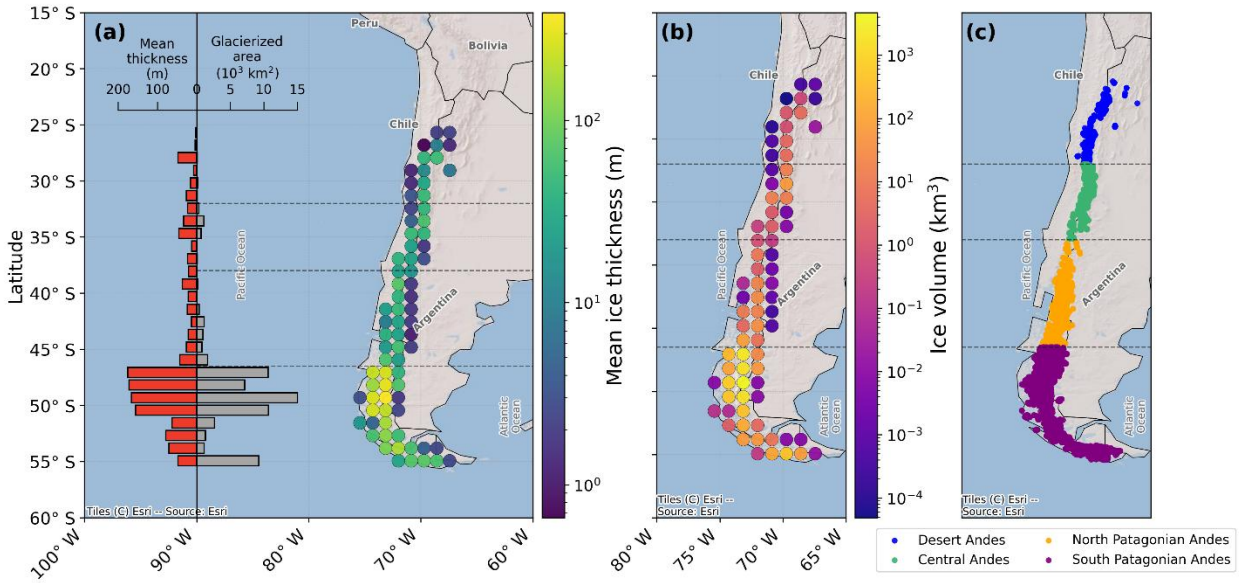


Table 1: Glacier number, ice thickness, ice volume and sea level equivalent (SLE) across the glacierised regions of the Southern Andes. SLE incorporated a flotation correction applied to marine terminating glaciers, excluding the ice grounded below sea level.

Region	Glacier Count (n)	Volume total (km^3)	Thickness mean (m)	SLE (mm)
Dry Andes	2,029	8,4 ± 2,99	31,3 ± 11,9	0,02 ± 0,008
Central Andes	3,807	77,46 ± 28,10	53,4 ± 20,2	0,19 ± 0,07
Northern Patagonian Andes	6,927	65,66 ± 22,4	38,08 ± 14,6	0,16 ± 0,05
Southern Patagonian Andes	17,871	5808,69 ± 1,927	247,95 ± 82,3	14,39 ± 4,78
Total	30,634	5960,20 ± 1,980	242,01 ± 73,7	14,76 ± 4,9

Bedrock maps and glacial lakes

Applying a minimum area threshold of 0.01 km^2 , we identify 3.951 potential future glacial lakes formation across the Southern Andes, representing a total potential water volume of 298.63km^3 (Table 2). Most of them are located in the Southern Patagonian Andes (3268) which hold 83% of all sites and 95% of the potential volume. This lake volume is almost entirely concentrated in the three Patagonian icefields (NPI, SPI, CDI) which store 247 km^3 across 2,131 sites. As for ice volume, the three large icefileds dominate the future potential for lake formation in terms of frecuency and volume. The numerous, smaller glaciers elsewhere, also in the other regions, play a secondary role.

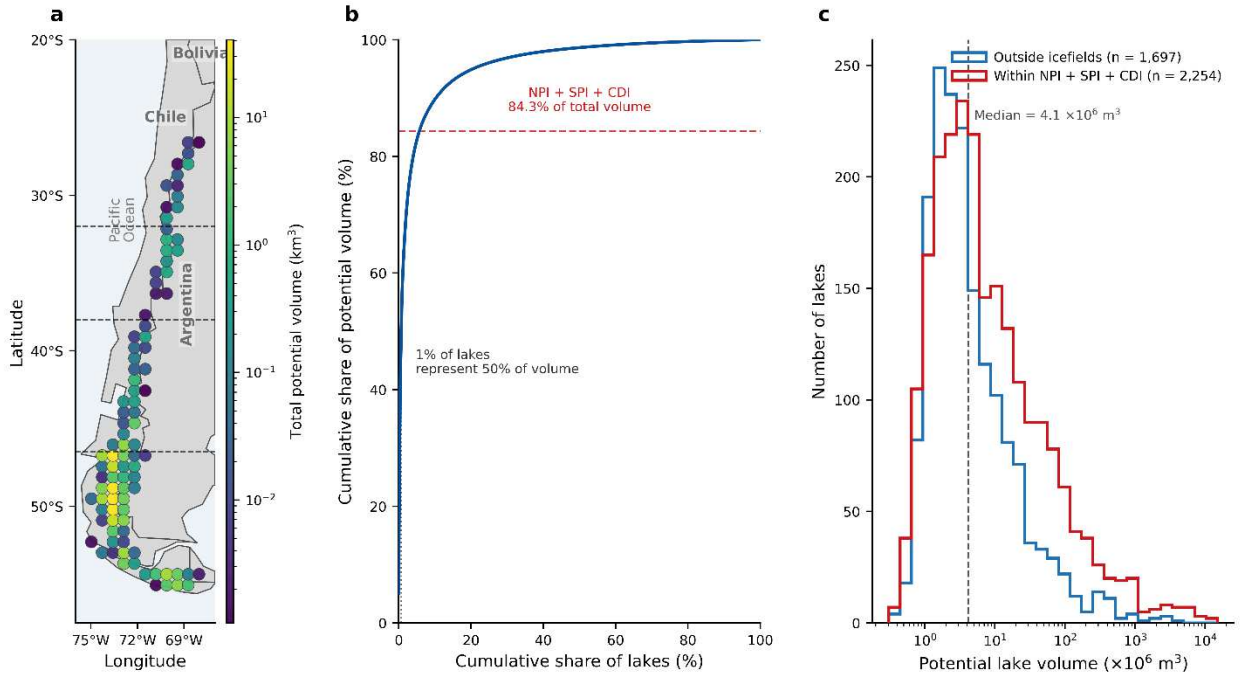
The volume distribution of all potential glacial lakes is strongly skewed by a few large currently ice-covered overdeepenings. This become evident by the mean and median pontial lake volume of $75.6\times10^6m^3$ and $4.1\times10^6m^3$, respectively. Moreover, less than 1% of all sites (0.7%) Will store more than half of the lakes water when all areas became ice-free. Lake volume increases southward and peaks in the Southern Patagonian Andes, mean lakes depth, however, does not follow this gradients, being comparable in the Northern (103 m) and Southern (101 m) Patagonian Andes and lower in the Central Andes (73 m).

Table 2: Summary statistics of potential lakes across the Southern Andes.

Region	Count (n)	Area cum. (km^2)	Vol. com. (km^3)	Depth Mean	Area Mean (km^2)
Dry Andes	64	17.6 ± 5.5	1.1 ± 0.17	79.9 ± 31.5	0.28
Central Andes	250	50.7 ± 18.7	2.7 ± 0.29	73.0 ± 29.2	0.20

Northern Patagonian Andes	369	110.0 ± 29.7	9.7 ± 0.65	103.3 ± 41.1	0.30
Southern Patagonian Andes	3268	2980.6 ± 431.1	285.0 ± 10.93	101.4 ± 33.1	0.91
NPI, SPI and CDI	2131	2587.8 ± 333.9	247.8 ± 10.6	101.4 ± 326	1.21
Outside Icefields	1137	392.8 ± 97.2	37.19 ± 2.36	101.5 ± 36.6	0.35
Total	3951	3158.8 ± 233.1	298.6 ± 10.9	99.4 ± 32.7	0.80

Figure 2: Potential future glacial lakes in the Southern Andes (a) Map of the potential water volume per cell, over the same ESRI World Shaded Relief Blackground and with the same regional boundaries. (b) Cumulative share of total lake volume as a function of the comulative share lakes. (c) Distribution of individual lake volume for lakes within the three icefields versus those outside them.



Water resources in future glacial lakes

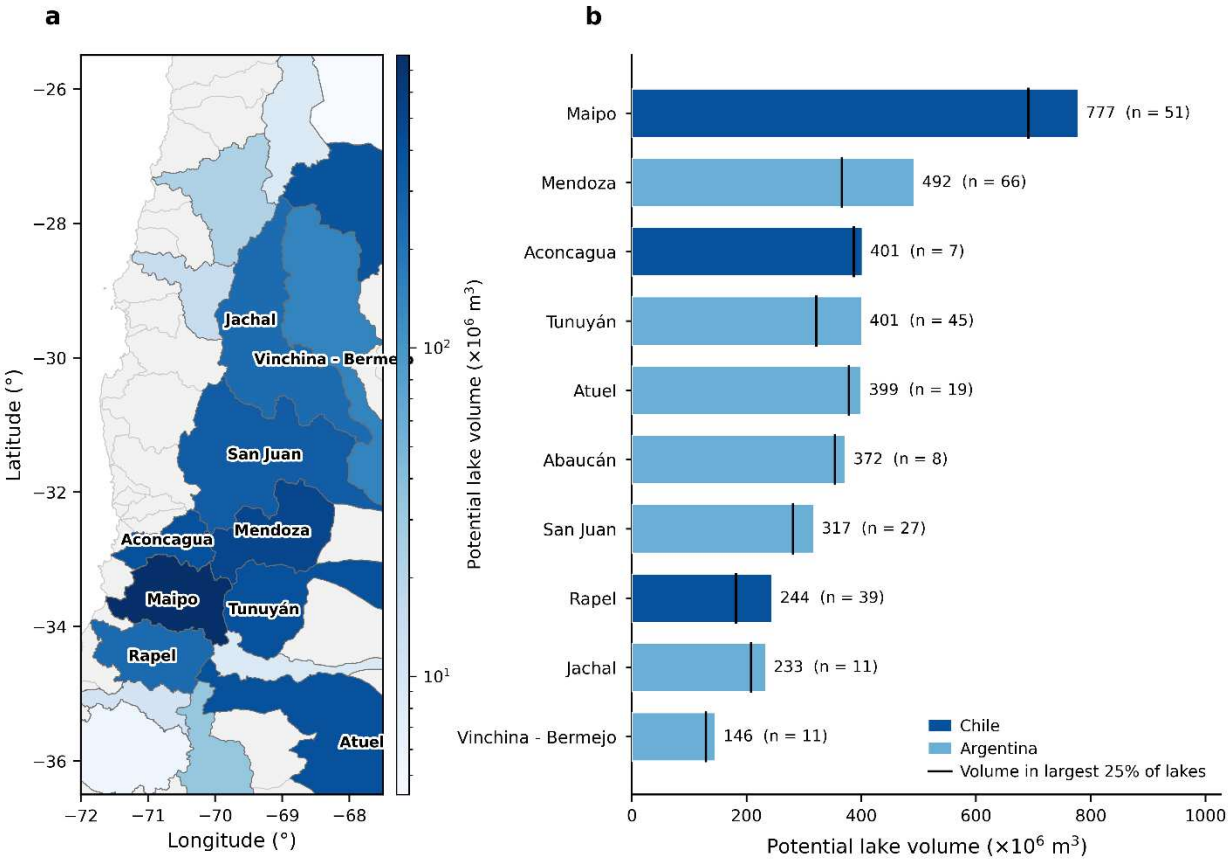
The Desert Andes and the Central Andes hold only a small share of the total potential glacial lakes volume ($3.89 \times 10^6 m^3$). Yet lakes there are of high strategic value in terms of water management. The reason is that the northern regions lie in the arid Desert Andes and the semi-arid to Mediterranean Central Andes, where glaciers are key to sustain river flow throughout the dry season. Water storage capabilities in future ice-free areas are highly estemed.

The main portion of future lakes volume water is concentrated in a small number of catchments central to the water supply on both sides of the Andes (Figure 3). In the Central Andes, the Río Maipo basin ranks first, with $777 \times 10^6 m^3$ of potential storage across 51 lakes (20% of the lakes in the Central Andes, holding ~28% of the regions potential volume) This basin is vital for the water resources of the Santiago metropolitan area, home to more than seven million people. The freshwater security strongly depends on seasonal snowmelt stored in reservoirs such as El Yeso. Such artificial reservoirs have been under pressure from the prolonged megadrought (Garreaud et al., 2020). Overdeepenings that turn ice-free during future glaciers demise hold an important potential for freshwater storage, comparable to the current existing infrastructure. The neighboring Río Aconcagua ($401 \times 10^6 m^3$) and Río Rapel ($244 \times 10^6 m^3$) basin support the Valparaíso region and the central Chilean agricultural valleys. On the Argentnian sides of the Central Andes, the Mendoza ($492 \times 10^6 m^3$), Tunuyán ($401\times 10^6 m^3$), Atuel ($399\times 10^6 m^3$), and San Juan ($317\times 10^6 m^3$) basins are the water towers that allow irrigation and viticulture in the local semi-arid climate. Also there, as substantial amount of potential water storage is identified.

In contrast, the Desert Andes to the north hold the smallest potential volume ($1.1\ km^3$) in the part of the region where water scarcity is most severe. This is only moderately below the Central Andes

(2.7 km^3), which is notable given that the Desert Andes contain roughly half as many lakes, the differences lies less in the total volume than in how it is distributed across basin.

Figure 3: Potential future glacial lake water resources in the Desert ande Central Andes (a) Hydrological basin coloured by the total potential volume of the future glacial lakes and (b) The 10 basins with ice largest potential lake volume.



Discussion

Estimates of glacier bed topography in the Southern Andes have so far relied on global-scale approaches, with limited regional constraints from thickness measurements (Linsbauer et al., 2012; Farinotti et al., 2019). Our model differs from these products in three respects, i.e. in the amount of ingested thickness measurements, the consideration of retreat information of land-terminating

glaciers and the attempt to quantify of associated, spatially distributed uncertainties. Validation against independent observations will serve to assess the quality of our estimates and earlier maps of ice-free basal topography.

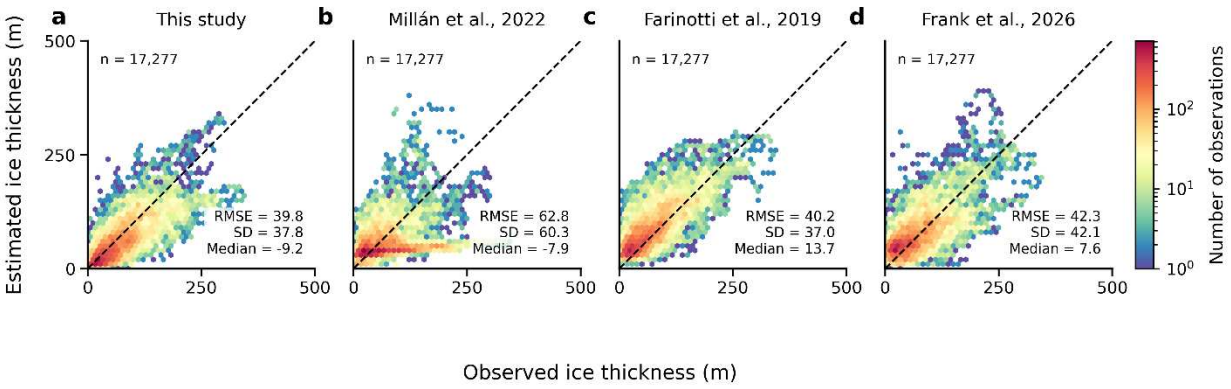
First, the yield stress was calibrated against 22186 thickness measurements collected along 695 km of radar profiles recently collected over 48 ice bodies (DGA, 2011; DGA, 2014; Koch et al., 2026). Most of this data has not been used in previous reconstructions. This record is complemented by thickness recors available for the Northern and Southern Patagonian Icefields (Fürst et al., 2024). Second, we used the terrain exposed by glacier retreat to constrain the bed near past extents of land-terminating glaciers, similar to Sommer et al. (2023), no other estimate available for the Southern Andes incorporated a comparable constraint from glacier retreat. Third, we provide a formal uncertainty map on the thickness distribution, following Koch et al. (2026) based on sensitivity experimets that primarily account for methodological decisions on yield stress extrapolation and the quality of the digital elevation model. Over the icefields, we rely on the existing thickness and uncertainty map by Fürst et al.(2024). A spatially distributed uncertainty map is no available for most existing products.

Performance against in-situ measurement

First, we compare the reconstruction thickness of our approach and three previous estimates (consensus estimated of Farinotti et al. 2019, Millan et al., 2022 and Frank et al., 2026) to the recent radar measurements. For a clean comparison, we re-ran our approach withholing these observations, admittedly, our results remain indirectly informed by them through the regional yield-stress values used for glaciers without measurements, so this comparison also gives some indication of the transferability of our approach. Over the 17,277 radar observations, for which all four products generated a value, our maps show an RMSE of 39.8 m, compared with the 40.2 m

consensus estimate (Farinotti et al,. 2019), 42.3 m for Frank et al. (2026), and 62.8 m for Millan et al. (2022) (Figure 4). This aggregate figure masks a regional pattern in which no single product predominates. In the dry Andes, our model performed worst out of the four, underestimating the measured thickness by 22.2 m in an area where the ice has an average thickness of only around 30 m (RMSE of 28.6, compared with 14.9 for Millan et al., 2022, based on the 226 available measurements). In the Central Andes consensus (Farinotti et al., 2019), the estimate shows a slight error (42.3 m compared with 44.4 m), and Frank et al. (2026) report the smallest bias (-1.8 m compared with -16.4 m). In the Andes of northern Patagonia, our maps are closer to the measurements across all parameters: an RMSE of 29.5 and a bias of –4.3, compared with 35.1 to 48.3 and +17.0 to +21.5 for the other three models. The full comparison for each area is presented in the Supplement. As these measurements form part of our calibration, our own agreement with them quantifies what a regional calibration achieves rather than testing it; the deviation of the other three models, which do not incorporate these data, is independent of that calibration.

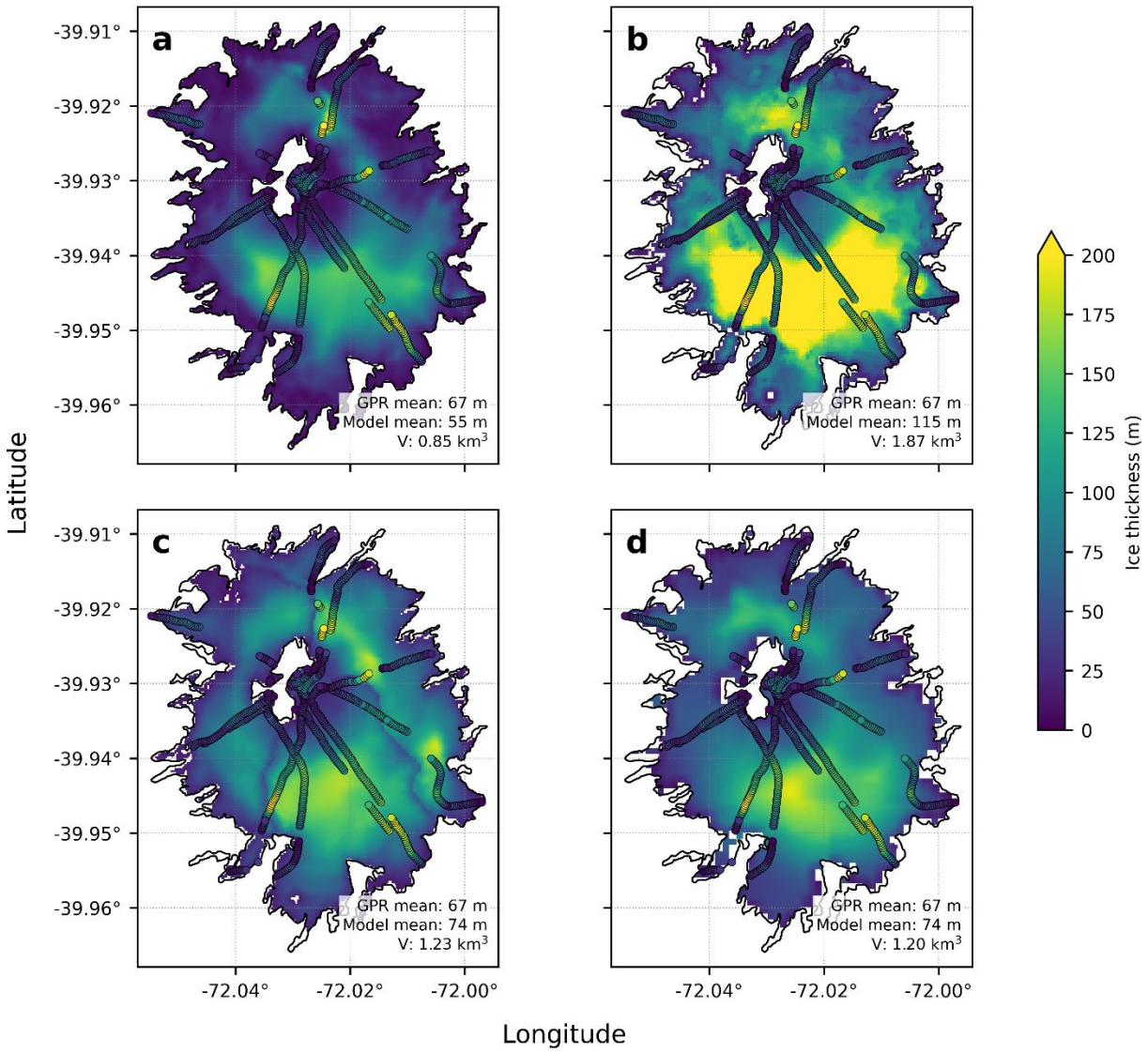
Figure 4: Modelled ice thickness against radar mesauramentes: Hexagonal binning of modelled against measured thickness for (a) This study, (b) Millan et al., 2022, (c) Consensus (Farinotti et al., 2019) and (d) Frank et al., (2026). Over the 17277 radar points at wich all four products return a value. Colour gives the number of observations per bin on a logarithmic scale, the solid line black is the 1:1 relationship.



266

267 Regardless of the similatiries in the bulk performance metric above substantial disagreements can
268 occur at the scale individual glaciers. This is important, as our interest lies in potential lakes sites
269 and thus in local bedrock topography. Here we showcase the Mocho-Choshuenco glacier complex
270 as an example with radar measurements. The various mapping attemps show mean thickness
271 values differ by more than a factore of two (Figure 5), raning from 55 m in our reconstruction, via
272 74 m in both Farinotti et al. (2019) and Frank et al. (2026) to 115 m in Millan et al., (2022).
273 Nonetheless, the spatial distribution of glacier ice thickness appears similar, Note that all previous
274 estimates were based on the RGI6, while our model use the updated RGI7 (RGI 7.0 Consortium,
275 2023).

276 **Figure 5: Modelled ice thickness at Mocho-Choshuenco. Thickness from (a) Our model, (b)**
277 **Millan et al. (2022), (c) Consensus (Farinotti et al., 2019) and (d) Frank et al. (2026).**



278

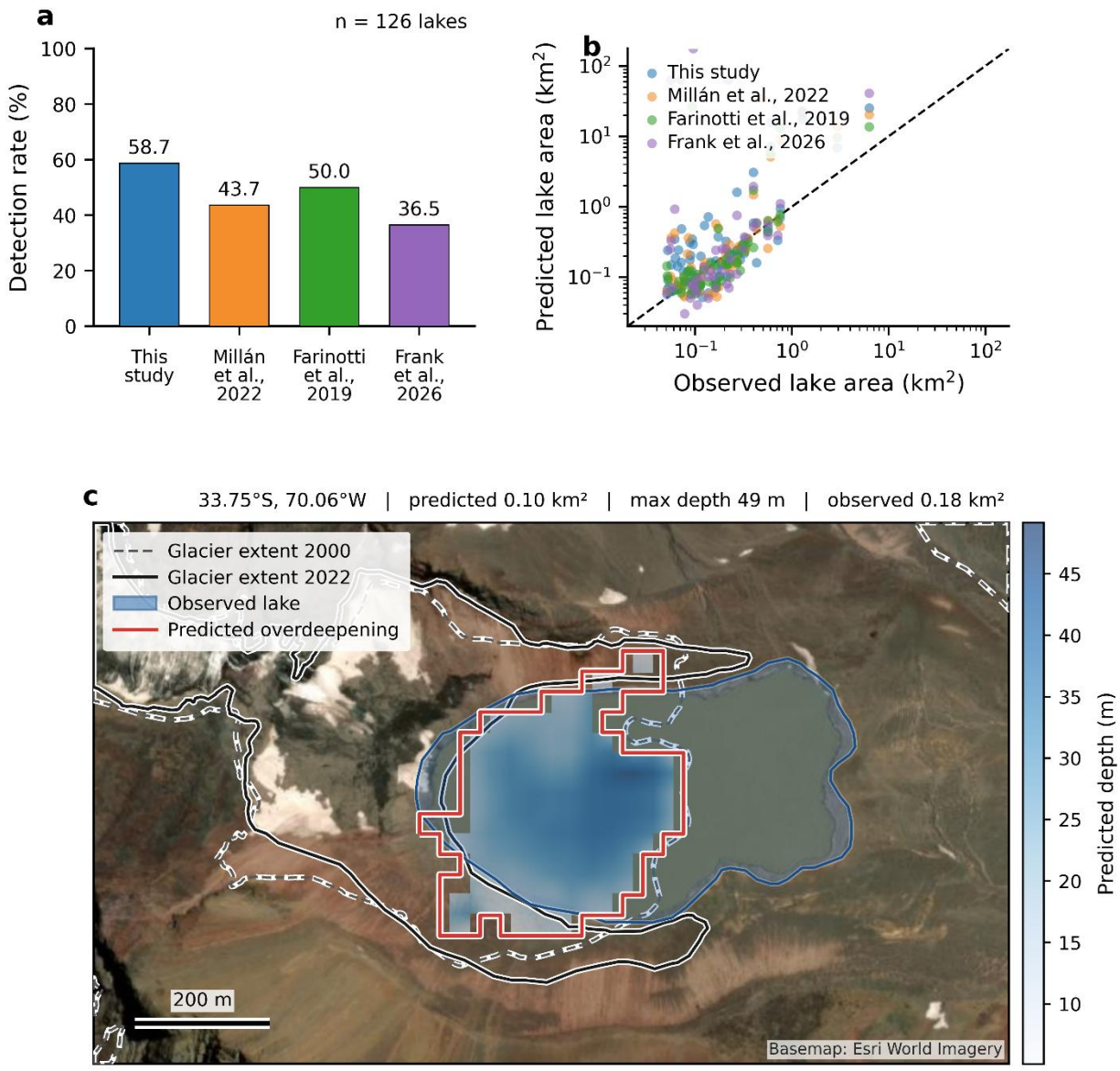
279 **Observed lake growth and expansion**

280 Many lakes have formed since 2000, the timestamp of the SRTM surface topography and therefore
281 of our thickness product. These new or expanding lakes provide of genuinely overdeepened
282 topography and thus offer an independent validation, following the approach applied in the
283 Himalayas (Furian et al., 2020). Og the 126 lakes observed in the deglaciated area between 2000
284 and 2022, our reconstruction recovers 58.7% by number (Figure 6a), an asset considergin that only
285 50% are reproduced by the consensus estimate (Farinotti et al., 2019), 43% by Millan et al.(2022)

and 36.5% by Frank et al. (2026). An example of observed lake growth occurred near Morado Glacier located in the Central Andes, close to Santiago de Chile (Figure 6c), where a lakes has grown within predicted overdeepening at a modelled depth of 49 m. Here the prediction is essentially exact, the observed lakes occupies a site our model correctly identifies as an overdeepening, and the fact that its current outline (0.18 km^2) already exceeds the ice free basin we resolve (0,10 km^2) reflects that roughly half of he lake had already formed before the reconstruction period.

Among the lakes that each products, our median intersection over union is 0,38 the lowest of the four (0.52 for Farinotti et al., 2019). Two factors explain this, First, the median are evaluated across different subset, our over 74 lakes against 63 for Farinotti et al. (2019), so the eleven additional lakes we recover are predominantly marginal cases that lower our median, while being missed entirely by the other products. Second, and more fundamentally, the observed lakes growth has in many places not yet advance enough to fill the entire possible topographic overdeepening, parts are still occupied by glacier ice. We therefore do not expect a full outline match, certainly not where lakes remain ice dammed. The interest here is rather to assess whether our predicted lakes sites match to some degree, those that have grown over the past decades, and for that purpose, recovering the site matters more than reproducing the outline it currently holds.

Figure 6: Observed proglacial lakes growth and predicted overdeepenings. (a) Detection rate, defined as the percentage of the 126 lakes observed on terrain deglaciated between 2000 and 2022. (b) Predicted against observed lake area for each product. (c) Example near to Morado Glacier in the Central Andes; the 2000 and 2022 glacier.



308

309 The projected elevation distribution of future glacial lakes tracks closely with ice volume, with
310 maxima in lakes occurrence at low to mid-elevations, especially bellow 2,000 m a.s.l
311 (Supplementary Fig S2). This pattern aligns with prior research, which shows that overdeepenigns
312 are primarly located at the lower reaches of glaciers, coinciding with peak ice thickness and basal
313 erosion rates (Pandit and Ramsankaran, 2020; Zhang et al., 2022; Furian et al., 2022). The marked

concordance between current and predicted lake locations suggests that landscape evolution will be dominated by the expansion and coalescence of existing water bodies.

Freshwater storage and sea level relevance

As the ice is lost, its water partitions into two states: a fraction is intercepted by the overdeepenings exposed by the retreat and remains stored on land, while the rest is exported downstream and ultimately to the ocean. The retained fraction is 298.6 ± 11.0 km^3 of potential glacial lakes storage, which is 5% of the 5960 km^3 of ice in the region (equivalent, in ice, to roughly 326 km^3). Not all of this is available as freshwater, however, part lies in basins that will be connect to the ocean and is therefore of no use for water storage. This retained share is significantly larger than reported for Himalayas-Karakoram, where potential future glacial lakes will reain only 3-4% of the present dat glacier volume (Linsbauer et al., 2016). Values are lower elsewhere too ~3% in the Swiss Alps (Linsbauer et al., 2016), the Aosta Valley to 0.8% (Vianni et al., 2020), and 0.5-1% in the Peruvian Andes (Colonia et al., 2017). Frank et al. (2026) obtain a comparable 5.9% for the Southern Andes from an independent reconstruction, against a global 2.1%. There is thus agreement that the deep, intensely eroded beds of the Patagonian Icefields can retain a notably high portion of water.

For sea level, the relevant quantity is how much of this ice actually raises the ocean, since only the volume above flotation contributes. Most of our potential lakes lie well inland, anove sea level, but 210 basin in the Southern Andes have floors below sea level, the ice occupying that space was already below sea level and never counted towerds sea level rise, Once this portion and the marine terminating flotation correction are accounted for, the volume above flotation that genuely contributes to sea level rise. This mirrors the mechaninsm Frank et al. (2026) identify globally, where interception by future lakes lowers the sea level equivalent of complete melt by about 2%,

the effect is proportionally larger here, in keeping with the regions unusually deep beds, and is resolved only once the basins are mapped.

Ice dynamics and comparison with other reconstrutions

Beyond their role as water stored and hazard sources, the overdeepening mapped here matther for glacier dynamics, particulary for the outlet glaciers of the large Southern Patagonian Icefields. Marine and lake terminating glaceirs that end in deep water retreat faster than their land terminating counterparts, the depth of the basin they occupy is itself a control, as low effective pressure over an overdeepening increases buoyancy, accelerates flow and promotes calving (Post et la., 2011). The clearest regional example is Glaciar Upsala, which retrat 2.9 km, accelerated by 20-50% and thinned at up to 39 m a^{-1} between 2008-2011 (Sakakibara et al., 2013), the onset of that retreat has been attributed to the terminus reaching a part of the lake deeper 560 m (Sugiyama et al., 2016). Comparable behaviour is documented at Jorge Montt glacier (Rivera et al., 2012) and at Marinelli, where the erosion raters during rapid retreat were roughly four times those of the stable phase (Koppes et al., 2009). Our reconstruction points to the section of future fjord and lake bathymetry along which are most likely to undergo self accelerated retreat.

The four estimates are based on different physical assumptions and observational data, and the discrepancies between them exhibit a reginoa pattern (Fig S1). Millan et al. (2022) invert surface velocities from satellite data and produce no estimate where usable velocities are absent, in the Dry Andes their maps show no value for 69% of the rader survey, so their volume there reflects incomplete coverage rather than a systematic underestimation of thickness. The consensus estimate of Farinotti et al., (2019) combines several approaches which smooths the subglacial topography and reduces the depth og the inferable overdeepenings. Our reconstruction diverges most from the other in the Northern Patagonian Andes, where we got 64 km^3 againts 77.4, 78.2

359 and 78.5 km^3 for Farinotti et al. (2019), Frank et al. (2026) and Millan et al., (2022), respectively.
360 A difference of 19% is notable given that these approach otherwise agree within 1.3% and the
361 radar record resolves it in favour of the lowest estimate, across the 5,797 measurements in this
362 area, the three studies overestimate the observed thickness by 17 to 21.5 m. wherears our bias is
363 4.3 (Fig 4; Fig S5). None of these three products was calibrated with these radar data, so their
364 excess volume corresponds directly to their excess thickness, this is also the area where our
365 ingested thickness recors are most abundant.

366 Frank et al. (2026) recently provided the first globally consistent reconstruction of glacier bed
367 topography, estimating a potential future lake volume of 408 km^3 for the Southern Andes, with an
368 average depth of 124 m. Evaluated over a common minimum lake area of 0.05 km^2, our reginal
369 estimate is 296.6 km^3 with a mena depth of 94.5 m, amounting to 73% and 76% of those values,
370 respectively. This difference stems almost entirely from the Southern Patagonian Andes, where
371 we obtain 285 km^3 against 397.9 km^3, in the remaining three zones our estimate exceeds theirs by
372 a factore of 3.2 in the Dry Andes and 1.5 in the Northern Patagonian Andes, and matches within
373 9% in the Central Andes. A primary explanation is the abundant thickness record not available to
374 Frank et al. (2026), secondary reasons are the choice of glacier outlines and methodological
375 differences. Nonetheless, both estimates agree that the Southern Andes area a global hotpost for
376 future glacial lakes formation.

377 ## Conclusion

378 We have reconstructed ice thickness in the year 2000 and, with it, unveiled the subglacial
379 topography across the entire Southern Andes, The motivation for updating existing maps is the
380 availability of recent radar measurements across Chile and the ingestion of information on past ice
381 thickness from ongoing glacier retreat. The benefit of these constraints is measurable, our maps

reproduce the radar measurements to a RMSE error of 39.8 m and recover 58.7% of the lakes that have formed on recently glacier free terrain, outperforming predecessor products. The reconstruction places the regional ice volume at 5,960 ± 1980 km^3, equivalaent, (after accounting for flotation), to 14.5 ± 4.99 mm of sea level rise. We further identify 3,951 potential sites for future glacial lakes formation, which can retain a total of 296.6 km^3 of water, about 5% of the current ice volume, this fraction is corroborated by a recent study and is exceptionally high when compared to other mountaing regions wordwide (Frank et al., 2026).

These results carry three implacations. First, our new volume estimates differ notably from existing products. This will affect not only future projections of glacier demise in Southern Andes, but also the rolo thse glaciers can play in the hydrological cycle -from their buffering function to peak-water and water tower concepts. Where the three existing products overestimate radar measured ice by 28 to 21 m, as they do throughout the Northern Patagonian Andes, placing 19% more ice than we do, that excess propagates directly into the volume of ever basin they predict and into any retreat simulation initialized from them, a bed calibrated to the measurements correct both at once.

Second, the future glacial lakes will partly alleviate the loss of the glacial landscape, forming new freshwater reservoirs of globally significant volume and of decisive local hydrological relevance, In the Central Andes, the potential storage we map is of the same order as the principal existing reservoirs of the Maipo basin, on which the water security of Santiago depends.

Third, the same beds determine where fast, self accelerating retreat and glacial lakes outburst flood are most likely to develop. A glacier whose terminus enters a deep lake retreats more rapidly than its land terminating counterparts, as at Upsala, where the onset of rapid retrat has been attributed to the front reaching water more than 560 m deep. By resolving the bathymetry of the lakes that

will be exposed, our mpas identigy in advance where these feedbacks and the outburst flood hazard that accompanies the deepest lakes are most likely to develop.

The inventory is a starting point, not a projection, It delimits the maximum extent each lake can attain once the ice has vanished, not the state of any lake at a given date, and it does not resolve the timing of formationor the sediment infilling that will reduce the final volume. Coupling these bed to transient glacier-evolution models. And to the sediment fluxes that will partly fill the basins, is the necessaty next step to turn a map of where lakes can form into an assessment of when they will form and what hazard they will pos. The regionally calibrated bed provided here is the observation foundation on wihcj that step can be built.

Methods

Data

To analyze ice thickness and potential future glacial lakes, we integrated satellite and field data. The Digital Elevation Model (DEM) used corresponds to the Shuttle Radar Topography (SRTM) with a 30-meter resolution, acquired between February 11 and 20 (Farr et al., 2007). This DEM was used to derive glacier-surface slopes and calculate the subglacial surface.

For the calibration of ice thickness, we employed GPR (DGA 2012-2014). These thickness measurements were collected over 48 ice bodies, covering approximately 695 km of radar profiles and comprising a total of 22,186 point measurements distributed across three main glaciological zones: Desert Andes, Central Andes, and Northern Patagonian Andes.

Remote sensing data-derived changes in glacier elevation and extent were used to infer past ice thickness in areas that have recently become ice-free (Sommer et al., 2023). To complement this

reconstruction, we also incorporated geodetic mass balance data obtained from elevation differences. Finally, glacier outlines were obtained from version 7 of the RGI and from the official Chilean glacier inventory of 2020.

Thickness estimation

Glacier ice thickness was estimated using the equations of perfect plasticity (Fürst et al., 2018), which assume that ice behaves as a plastic material that flows downslope. Under this approach, ice begins to deform once the basal stress exceeds a critical threshold, known as the yield stress (Fürst et al., 2018). These equations have been used to estimate the spatial distribution of thickness in mountain glaciers (Frey et al., 2014, Fürst et al., 2018), particularly in regions where in situ data are scarce (Linsbauer et al., 2012).

The fundamental equation of the perfect plasticity model relates the ice thickness (H) to the yield stress (τ_y) and the surface slope ($|\nabla h|$), as shown below:

$$H = \frac{\tau_y}{\rho g \, |\nabla h|}$$

Where, H: Ice thickness (meters), τ_y is the Yield stress (Pa), the critical stress required for the ice to begin flowing , ρ: Ice density (910 kg/m^3, Cuffey and Paterson),g: Gravitational acceleration (m/s^2) and $|\nabla h|$ surface slopes, which are the gradient of the glacier surface elevation. These surface slopes ($|\nabla h|$) is derived from the spatial variation in surface elevation using the following expression:

$$|\nabla h| = \sqrt{\left(\frac{\partial h}{\partial x}\right)^2 + \left(\frac{\partial h}{\partial y}\right)^2}$$

The surface slopes were derived from SRTM using centered differences between adjacent cells. We implemented the approach developed by Fürst et al. (2018) within the numerical framework of the Elmer/Ice model (Gagliardini et al., 2013), which solves the glacier flow equation using the finite element method. The perfect plasticity equation was formulated as a condition of equilibrium between the gravitational driving stress. Elmer/Ice allows for the incorporation of glacier outline, DEMs, and spatially distributed physical parameters as inputs, and the glaciological community widely uses it for studies of ice thickness, glacier dynamics, and long-term evolution.

Yield Stress (τ_y)

The yield stress (τ_y) represent the critical stress required for the ice to deform plastically. In this study, τ_y was estimated using two main types of data: (I) direct ice thickness measurements obtained from GPR and (II) geodetic mass balance derived from multi-temporal surface elevations.

In locations where ice thickness data were available, the following equation was used to derive the yield stress:

$$\tau_y = \rho g h \sin(\alpha)$$

Where h is the ice thickness measurements (meters) and $\sin(\alpha)$ the surface slope (radians). However, for glaciers where neither GPR measurements nor reateat data were available, we applied an alternative empirical parameterization to estimate the basal yield stress (Haeberli and Hoelzle, 1995)

$$\tau_{y0} = \begin{cases} 0.5 + 159.8\Delta H - 43.5(\Delta H)^2 & , \Delta H \leq 1.6 \\ 150 & , \Delta H > 1.6 \end{cases}$$

The model was calibrated and parameterized to adjust the basal yield stress (τ_y), a critical parameter for estimating ice thickness based on the mechanical equilibrium of a glacier. An initial value (τ_y) was estimated in areas where glaciers retreat, with the assumption that loss of ice thickness (dh/dt). In these regions, it indicates the beginning of ice flow.

The initial yield stress(τ_{y0}) value was further refine for each glacier drainage basin as a 2D map. Therefore, a spatial scaling was implemented to account for topographic factors. The scaled yield stress is calculated using the following equation:

$$\tau_y = \tau_{y0} \cdot \xi^{\tau}_{\text{slope}} \cdot \xi^{\tau}_{\text{elevation}} \cdot \xi^{\tau}_{\text{distance}}$$

Where τ_{y0} corresponds to initial yield stress value, $\xi^{\tau}_{\text{slope}}$ the correction factor for slope, $\xi^{\tau}_{\text{elevation}}$ the correction factor for elevation, and, $\xi^{\tau}_{\text{distance}}$ the correction factor accounting the distance to the glacier margin (cf. Sommer et al. (2023)). The slope correction factor is defined as:

$$\xi^{\text{slope}}_{\tau_y} = \xi^{\text{slope, 0}}_{\tau_y} \cdot \left(\alpha - \alpha^{\text{thres}}_{\tau_y}\right)$$

Where α is thelocal slope and $\alpha^{\text{thres}}_{\tau_y}$ the threshold angle beyond which the correction is applied.

The elevation factor is applied using the normalized elevation $\hat{h}$ of the glacier:

$$\xi^{\text{elevation}}_{\tau_y} = 1 + \gamma^{\text{elevation}}_{\tau_y} \cdot \left(\hat{h} - \widehat{h^{\text{thres}}_{\tau_y}}\right)$$

This correction reduces τ_y in areas with very high elevation where the glacier is often flatter, and increases it in lower areas where the flow is more intense.

Finally, the distance factor accounts for the position of the pixel within the glacier. It is defined as follows:

$$\xi_{\tau_y}^{\text{distance}} = \tan^{-1}\left(\frac{d_{\text{margin}}}{4 \cdot H}\right) \cdot \frac{2}{\pi}$$

Where d_{margin} is the distance to the glacier margin and H is the estimated ice thickness.

This correction reduces stress near the margin where edge effects influence deformation.

Uncertainty Analysis of the ice thickness model

To estimate the error in the ice thickness reconstruction associated with the parametrization of yield stress (τ_y), we perform a sensitivity analysis focused on a set of influence variable and parameters. To do this, we follow and modify the uncertainty approach proposed by Koch et al. (2025), who estimated the ice thickness error based on the calculation of the mean absolute deviation.

Unlike Koch et al., (2025) where the uncertainty is evaluated using the effective viscosity of the ice, in our model, we calculated the error by perturbing the yield stress (τ_y), which is the only mechanical parameter in the model.

A reference ice thickness $H_r(x)$ was calculated using the yield stress distribution considered to be the best estimate ($\tau_{y(REF)}$), Subsequently, additional simulations were generated by uniformly perturbing the yield stress field by ±10%, ±15%, and ±20%, representing a plausible range of error.

Let $HE_i(x)$ be the ice thickness obtained in the i-th perturbed simulation with i=1.. N and N=6. The error associated with the yield stress was defined following Koch et al., (2025) as the mean absoluted point to point deviation between the different ice thicknesses with yield stress.

$$U_{\tau_y}(x) = \frac{1}{N}\sum_{i=1}^{N}\left|H_r(x) - HE_i(x)\right|$$

In addition to the uncertainty associated with yield stress, the uncertainty with the DEM was incorporated. We used the SRTM DEM as input topography. Global assessments of SRTM indicate that the absolute error in South America is approximately 6.2 meters, while the relatively high error is close to 5.5 meters (Rodriguez et al., 2006; Farr et al.,2007). Therefore, we use a value of ±6 meters as the vertical uncertainty of the DEM.

$$U_{DEM}(x) = 6\ \text{m}$$

Assuming independence between the yield-stress and the DEM uncertainty, the combined uncertainty associated with ice thickness was obtained using the quadratic propagation of errors

$$U_{total}(x) = \sqrt{U_{\tau_y}(x)^2 + U_{DEM}(x)^2}$$

Finally, to obtain a representative value of uncertainty at the glacier scale, the spatial field of error was integrated using an area-weighted average:

$$\overline{U}_{total} = \frac{\sum_x U_{total}(x)A_x}{\sum_x A_x}$$

Where A corresponds to each pixel

Identification of potential future glacial lakes

The identification of potential areas for glacial lakes formation was based on the analysis of closed depressions in the subglacial topography (Furian et al., 2021; Frank et al., 2026), under the hypothesis that overdeepening caused by glacial erosion can be filled with water once the ice has completely retreated. This approach has been proposed and validated across various glaciological areas worldwide, particularly in Europe (Linsbauer et al., 2012) and High Mountain Asia (HMA)(Furian et al., 2021). This approach is a hydrologically consistent, computationally efficient method for estimating the spatial distribution and volume of future glacial lakes under climate change.

Following the methodology proposed by Furian et al.(2021), a digital elevation model "without ice" was generated by subtracting the model ice thickness H(x,y) from the DEM $Z_{dem\,(x,y)}$.

$$Z_{bed}(x,y) = Z_{DEM}(x,y) - H(x,y)$$

This procedure enables us to reconstruct the basal topography currently obscured by ice, thereby eliminating the glaciers topographic effect. The accuracy of Z_{bed} depends directly on the quality of the ice thickness model and the DEM used. In this study, both products were topographically corrected and aligned to avoid matrix mismatches, ensuring geometry consistency for the analysis. A hydrological filling algorithm (FillDepressions) (Lindsay, 2016) was applied to the Z_{bed} surface, identifying and eliminating local sinks to generate a hydrologically consistent surface $Z_{filled\,(x,y)}$. The result of the filling corresponds to the maximum elevation at which an overdepeening could hold water without overflowing. The potential water depth in each cell is calculated as the difference between the filled model and the original bed.

$$D(x,y) = Z_{filled}(x,y) - Z_{bed}(x,y)$$

Map $D_{(x,y)}$ represents the theoretical bathymetry of possible lakes (Furian et al., 2021), expressed in meters. This procedure allows us to distinguish potential areas for glacial lakes formation and exclude artifacts derived from topographic noise or erroneous interpolations.

To avoid identifying unstable or unrealistic depressions, the criteria proposed by Furian et al. (2021) based on minimum depth and local slope, were applied:

$$D(x,y) = \begin{cases} D(x,y), & D(x,y) \geq 5\,\text{m and } \tan\left(|\nabla Z_{\text{filled}}(x,y)|\right) < 10^{\circ} \\ 0, & \text{(not lake).} \end{cases}$$

Where: $|\nabla Z_{\text{filled}}(x,y)|$ corresponds to the local slope calculated on the filled surface. The minimum value of 5 meters ensures that only depressions deep enough to retain water are considered. At the same time, the 10-degree slope threshold excludes areas with high roughness or unstable slopes where lake formation is unlikely

Lake delimitation and calculations of volume

Pixels with D(x,y) >0 were grouped into connected regions to define individual potential lakes (Ωk). The lakes were analyzed independently to estimate their morphometric and volumetric properties.

For each over-deepening k1, the outlet point (outlet) was identified as the cell with the lowest elevation at the edge of the polygon. This helps us determine the lake's maximum fill level, thereby avoiding overestimating its depth and volume. The fill is considered uniform up to that level, representing a first-order estimate of the volume, following Furian et al. (2021) procedure.

To qualify the geometric properties of each overdeepening, we computed total lake area, volume, maximum depth, and mean depth using standard equations. The lake area A_k was obtained as the product of the number of pixels within each depression N_k and the pixel area A_{pix}.

$$A_k = N_k \cdot A_{\text{pix}}$$

The potential lake volume V_k was calculated by summing the depth values $D'(x_i, y_i)$ for all pixels belonging to the depression Ωk multiplied by the pixel area:

$$V_k = \sum_{(x_i,y_i)\in\Omega_k} D'(x_i, y_i)\ A_{\text{pix}}$$

The maximum lake depth $D_{max,k}$, correspond to the maximum value of the filled depth grid $D'(x, y)$, within the polygon of each depression:

$$D_{max,k} = \max_{(x,y)\in\Omega_k} D'(x, y)$$

Finally, the mean lake depth $\overline{D_k}$ was computed as the average of all depth values within the depression, normalized by the total of pixels N_k

$$\overline{D_k} = \frac{1}{N_k} \sum_{(x_i,y_i)\in\Omega_k} D'(x_i, y_i)$$

Uncertainty Analysis of the future glacial lake

The uncertainty in estimating the volume of a future glacial lake was assessed using error propagation, considering uncertainties in the lake area and the estimated depth of subglacial

overdeepening. The relative uncertainty of the volume was estimated using the following equation (Pandit and Ramsankaran, 2020)

$$\frac{\Delta V}{V} = \sqrt{\left(\frac{\Delta A}{A}\right)^2 + \left(\frac{\Delta H}{H}\right)^2}$$

Where V is the volume of the lake, A is the area of the lake, and H corresponds to the uncertainties associated with area and depth, respectively. For each lake, a single relative depth uncertainty was obtained by integrating the ice thickness error map over the lake

$$\frac{\Delta H}{H} = \frac{\sum_{x \in \Omega_k} H_{u_total}(x)}{\sum_{x \in \Omega_k} H_{ice}(x)}$$

Where H_{u_total} are the per-pixel thickness error and the reconstruction H_{ice} of the ice thickness at the same point, both from the error analysis of the ice thickness model. Since H_{u_total} it is, by construction, a fraction of the local ice thickness, this ratio yields one bounded relative uncertainty per lake, rather than a pixel-wise one, applying the relative thickness error coherently over the lake's area.

Validation against observed lakes growth

To assess how well the predicted overdeepenings anticipate real lake formation, we compared them against lakes that have appeared or expanded in terrain that become ice free between 2000 and 2022. This reference set comprises 126 observed lakes located in areas that ice-covered at the SRTM (2000) and deglaciated by 2022.

589 Two complementary metrics were computed, applied identically to our reconstruction and to the
590 three comparison products (Farinotti et al., 2019; Millan et al., 2022; Frank et al., 2026).

591 First, the detection rate, defined as the fraction of the 126 observed lakes that spatially coincide
592 with a predicted overdeepening. An observed lakes was counted as detected when its polygon
593 intersected a predicted polygon.

594 Second, the intersection over union (IoU). For each detected lake, the spatial agreement between
595 the observed outline O and the predicted overdeepening P was estimated as

596 $$IoU = \frac{\text{area}(O \cap P)}{\text{area}(O \cup P)}$$

597 ## Sea-Level equivalent (SLE)

598 To estimate the Sea-Level Equivalent (SLE), we first calculate the total ice volume in cubic
599 kilometers

600 $$V = \frac{\sum h_i \times psx \times psy}{1 \times 10^9}$$

601 Where psx and psy correspond to the pixel size in meters, hi is the ice thickness located in each
602 pixel. Next, we consider the ice above the flotation level to obtain the volume of water.

603 $$V_{af} = V_{total} \frac{\rho_{ice}}{\rho_{water}} - V_{bsl}$$

604 Where V_{af} is the volume of water above floatation, $V_{total:}$ Total ice volume, ρ_{ice}: Density of the
605 ice (0.9167 Gt km^{-3}), ρ_{water}: Density of seawater (1.027 Gt km^{-3}), V_{bsl} is the volume located

606 below sea level using the geopotential model EGM96 as reference.Finally, the volume was
607 converted to SLE using the volume of ice needed to raise the global sea level by 1 mm.

608 $$SLE_{mm} = \frac{V_{af}\ \rho_{water}}{361.8}$$

609 ## Code Availability

610 Pertinent code for the reconstruction is available from GitHub at https://github.com/ FAU-glacier-
611 systems/ElmerIce_Thickness_Reconstruction.

612 ## References

613 1. Xu J, Grumbine, R.E., Shrestha A, Eriksson, M., Yang, X., Wang, YUN., Wilkes. A., (2009). The
614 melting Himalayas: cascading effects of climate change on water, biodiversity, and livelihoods.
615 Conserv Biol 23(3):520–530.

616 2. Carrivick, J.L. & Tweed, F.S. Proglacial lakes: character, behaviour and geological importance. *Quat.*
617 *Sci. Rev.* 78, 34–52 (2013). https://doi.org/10.1016/j.quascirev.2013.07.028

618 3. Shugar, D.H., Burr, A., Haritashya, U.K., Kargel, J.S., Watson, C.S., Kennedy, M.C., Bevington, A.R.,
619 Betts, R.A., Harrison, S., Strattman, K., 2020. Rapid worldwide growth of glacial lakes since 1990.
620 Nat. Clim. Chang. 10 (10), 939–945. https://doi. org/10.1038/s41558-020-0855-4.

621 4. Frank, T., van Pelt, W.J.J., Rounce, D.R. et al. Global glacier-free topography reveals a large potential
622 for future lakes in presently ice-covered terrain. Nat Commun 17, 3985 (2026).
623 https://doi.org/10.1038/s41467-026-72548-9

624 5. Iribarren Anacona, P., Mackintosh, A. & Norton, K.P. Hazardous processes and events from glacier
625 and permafrost areas: lessons from the Chilean and Argentinean Andes. *Earth Surf. Process. Landf.*
626 40, 2–21 (2015). https://doi.org/10.1002/esp.3524

627 6. Carrivick, J. L., Davies, B. J., James, W. H. M., Quincey, D. J. & Glasser, N. F. Distributed ice
628 thickness and glacier volume in southern South America. *Glob. Planet. Change* **146**, 122–132 (2016)

7. Furian, W., Loibl, D. & Schneider, C. Future glacial lakes in High Mountain Asia: an inventory and assessment of hazard potential from surrounding slopes. *J. Glaciol.* 67, 653–670 (2021). https://doi.org/10.1017/jog.2021.18

8. Immerzeel, W.W., Lutz, A.F., Andrade, M., Bahl, A., Biemans, H., Bolch, T., Hyde, S., Brumby, S., Davies, B.J., Elmore, A.C., Emmer, A., Feng, M., Fern´andez, A., Haritashya, U., Kargel, J.S., Koppes, M., Kraaijenbrink, P.D.A., Kulkarni, A.V., Mayewski, P.A., Nepal, S., Pacheco, P., Painter, T.H., Pellicciotti, F., Rajaram, H., Rupper, S., Sinisalo, A., Shrestha, A.B., Viviroli, D., Wada, Y., Xiao, C., Yao, T., Baillie, J.E.M., 2020. Importance and vulnerability of the world's water towers. Nature 577 (7790), 364–369.

9. RGI Consortium. (2023). Randolph Glacier Inventory - A Dataset of Global Glacier Outlines. (NSIDC-0770, Version 7). [Data Set]. Boulder, Colorado USA. NASA National Snow and Ice Data Center Distributed Active Archive Center. https://doi.org/10.5067/F6JMOVY5NAVZ. [describe subset used if applicable]. Date Accessed 08-17-2026.

10. Masiokas, M. H., Rivera, A., Espizua, L. E., Villalba, R., Delgado, S. & Aravena, J. C. Glacier fluctuations in extratropical South America during the past 1000 years. *Palaeogeogr. Palaeoclimatol. Palaeoecol.* **281**, 242–268 (2009).

11. Sagredo, E., and Lowell, T. (2012). Climatology of Andean glaciers: a framework to understand glacier response to climate change. Glob. Planet. Chang. 86–87, 101–109. doi: 10.1016/j.gloplacha.2012.02.010.

12. Caro, A., Condom, T. & Rabatel, A. Climatic and morphometric explanatory variables of glacier changes in the Andes (8–55°S): new insights from machine learning approaches. *Front. Earth Sci.* **9**, 713011 (2021).

13. Dussaillant, I., Berthier, E., Brun, F., Masiokas, M., Hugonnet, R., Favier, V., Rabatel, A., Pitte, P., Ruiz, L. (2019). South American Andes elevation changes from 2000 to 2018. Nature Geoscience, 12(10), 802-808.

14. Minowa, M., Schaefer, M., Sigiyama, S., Sakakibara, D., Skvarca, P. (2021) Frontal ablation and mass los of the Patagonian icefields. Earth and Planetary Science Letters, 561.

15. Braun, M. H., Malz, P., Sommer, C., Farías-Barahona, D., Sauter, T., Casassa, G., Alvarado., S, Svarca, P., Seehaus, T. (2019). Constraining Glacier Elevation and Mass Changes in South America. Nat. Clim Change 9 (2), 130–136. doi:10.1038/s41558-018-0375-7

16. Hugonnet, R., McNabb, R., Berthier, E., Menounos, B., Nuth, C., Girod, L., Farinotti, D., Huss, M., Dussaillant, I., Brun, F., Kääb, A., 2021. Accelerated global glacier mass loss in the early twenty-first century. Nature 592 (7856), 726–731. http://dx.doi.org/10.1038/s41586-021-03436-z

17. The GlaMBIE Team. Community estimate of global glacier mass changes from 2000 to 2023. Nature 639, 382–388 (2025). https://doi.org/10.1038/s41586-024-08545-z

18. Koppes M, Hallet B, Rignot E, Mouginot J, Wellner JS, Boldt K. Observed latitudinal variations in erosion as a function of glacier dynamics. Nature. 2015 Oct 1;526(7571):100-3. doi: 10.1038/nature15385. PMID: 26432248.

19. Garreaud RD, Boisier JP, Rondanelli R, Montecinos A, Sepúlveda HH, Veloso-Aguila D. The Central Chile Mega Drought (2010–2018): A climate dynamics perspective. Int J Climatol. 2020; 40: 421–439. https://doi.org/10.1002/joc.6219

20. McCarthy, Michael & Meier, Fabienne & Fatichi, Simone & Stocker, Benjamin & Shaw, Thomas & Miles, Evan & Dussaillant, Ines & Pellicciotti, Francesca. (2022). Glacier Contributions to River Discharge During the Current Chilean Megadrought. Earth's Future. 10. 10.1029/2022EF002852.

21. Huss, M., Hock, R. Global-scale hydrological response to future glacier mass loss. Nature Clim Change 8, 135–140 (2018). https://doi.org/10.1038/s41558-017-0049-x

22. GlaThiDa Consortium (2020): Glacier Thickness Database 3.1.0. World Glacier Monitoring Service, Zurich, Switzerland. DOI: 10.5904/wgms-glathida-2020-10

23. Fürst, J. J., Navarro, F., Gillet-Chaulet, F., Huss, M., Moholdt, G., Fettweis, X., Lang, C., Seehaus, T., Ai, S., Benham, T. J., Benn, D. I., Björnsson, H., Dowdeswell, J. A., Grabiec, M., Kohler, J., Lavrentiev, I., Lindbäck, K., Melvold, K., Pettersson, R., Rippin, D., Saintenoy, A., Sánchez-Gámez, P., Schuler, T. V., Sevestre, H., Vasilenko, E. & Braun, M. H. The ice-free topography of Svalbard. *Geophys. Res. Lett.* **45**, 11,760–11,769 (2018).

24. Farinotti, D., Huss, M., Fürst, J. J., Landmann, J., Machguth, H., Maussion, F. & Pandit, A. A consensus estimate for the ice thickness distribution of all glaciers on Earth. *Nat. Geosci.* **12**, 168–173 (2019).

25. Linsbauer, A., Paul, F., Haeberli, W. (2012). Modeling glacier thickness distribution and bed topography over entire mountain ranges with GlabTop: Application of a fast and robust approach. Journal of Geophysical Research: Earth Surface, 117(F3), n/a n/a. doi:10.1029/2011jf002313

26. Frey, H., Machguth, H., Huss, M., Huggel, C., Bajracharya, S., Bolch, T., Kulkarni, A., Linsbauer, A., Salzmann, N., and Stoffel, M.: Estimating the volume of glaciers in the Himalayan–Karakoram region using different methods, The Cryosphere, 8, 2313–2333, https://doi.org/10.5194/tc-8-2313-2014, 2014.
Wilson, R., Glasser, N. F., Reynolds, J. M., Harrison, S., Iribarren Anacona, P., Schaefer, M. & Shannon, S. (2018). Glacial lakes of the Central and Patagonian Andes. Global and Planetary Change, 162, 275–291. https://doi.org/10.1016/j.gloplacha.2018.01.004.

27. Iribarren Anacona, P., Mackintosh, A., Norton, K. (2015). Reconstruction of a glacial lake outburst flood (GLOF) in the Engaño Valley, Chilean Patagonia: Lessons for GLOF risk management. Science of the Total Environment, 527-528, 1-11.

28. Emmer, A. (2017). Glacier Retrat and Glacial Lake Outburst Floods (GLOFs). DOI:10.1093/acrefore/9780199389407.013.275

29. Huss, M. & Farinotti, D. Distributed ice thickness and volume of all glaciers around the globe. J. Geophys. Res. 117, F04010 (2012)

30. Maussion, F., Butenko, A., Champollion, N., Dusch, M., Eis, J., Fourteau, K., Gregor, P., Jarosch, A. H., Landmann, J., Oesterle, F., Recinos, B., Rothenpieler, T., Vlug, A., Wild, C. T. & Marzeion, B. The Open Global Glacier Model (OGGM) v1.1. *Geosci. Model Dev.* **12**, 909–931 (2019).

31. Millan, R., Mouginot, J., Rabatel, A. & Morlighem, M. Ice velocity and thickness of the world's glaciers. *Nat. Geosci.* **15**, 124–129 (2022).

32. Sommer, C., Fürst, J. J., Huss, M. & Braun, M. H. Constraining regional glacier reconstructions using past ice thickness of deglaciating areas – a case study in the European Alps. *The Cryosphere* 17, 2285–2303 (2023).

33. Koch, M., Sommer, C., Blindow, N. et al. The state and fate of Glaciar Perito Moreno Patagonia. Commun Earth Environ 6, 572 (2025). https://doi.org/10.1038/s43247-025-02515-7.

34. Koch, M., Berkhoff, J., Blindow, N., Farías-Barahona, D., Skvarca, P., Fürst, J. J. & Braun, M. Bedrock topography and ice thickness distribution of three major Patagonian outlet glaciers unveiled by helicopter-borne ground penetrating radar. Earth Syst. Sci. Data Discuss. [preprint], https://doi.org/10.5194/essd-2025-678 (2026).

35. Fürst, J. J., Farías-Barahona, D., Blindow, N., Casassa, G., Gacitúa, G., Koppes, M., Lodolo, E., Millan, R., Minowa, M., Mouginot, J., Pętlicki, M., Rignot, E., Rivera, A., Skvarca, P., Stuefer, M., Sugiyama, S., Uribe, J., Zamora, R., Braun, M. H., Gillet-Chaulet, F., Malz, P., Meier, W. J.-H. & Schaefer, M. (2024). The foundations of the Patagonian icefields. Communications Earth & Environment, 5, 142. https://doi.org/10.1038/s43247-023-01193-7

36. Farinotti, D., Brinkerhoff, D. J., Clarke, G. K. C., Fürst, J. J., Frey, H. *et al.* How accurate are estimates of glacier ice thickness? Results from ITMIX, the Ice Thickness Models Intercomparison eXperiment. *The Cryosphere* 11, 949–970 (2017).

37. Pandit, A. & Ramsankaran, R. Identification of potential sites for future lake formation and expansion of existing lakes in glaciers of Chandra Basin, Western Himalayas, India. *Front. Earth Sci.* 8, 500116 (2020).

38. Zhang, T., Wang, W., An, B., Gao, T. & Yao, T. Ice thickness and morphological analysis reveal the future glacial lake distribution and formation probability in the Tibetan Plateau and its surroundings. *Glob. Planet. Change* 216, 103923 (2022)

39. Furian, W., Maussion, F. & Schneider, C. (2022). *Projected 21st-Century Glacial Lake Evolution in High Mountain Asia*. Frontiers in Earth Science, 10, 821798. https://doi.org/10.3389/feart.2022.821798

40. Linsbauer A, Frey H, Haeberli W, Machguth H, Azam MF, Allen S. Modelling glacier-bed overdeepenings and possible future lakes for the glaciers in the Himalaya—Karakoram region. Annals of Glaciology. 2016;57(71):119-130. doi:10.3189/2016AoG71A627.

41. Viani, C., Machguth, H., Huggel, C., Godio, A., Franco, D., Perotti, L., Giardino, M., 2020. Potential future lakes from continued glacier shrinkage in the Aosta Valley Region (Western Alps, Italy). Geomorphology 355. https://doi.org/10.1016/j. geomorph.2020.107068.

42. Colonia, D., Torres, J., Haeberli, W., Schauwecker, S., Braendle, E., Giraldez, C., & Cochachin, A. (2017). Compiling an Inventory of Glacier-Bed Overdeepenings and Potential New Lakes in De-Glaciating Areas of the Peruvian Andes: Approach, First Results, and Perspectives for Adaptation to Climate Change. Water, 9(5), 336. https://doi.org/10.3390/w9050336

43. Sakakibara, D., Sugiyama, S., Sawagaki, T., Marinsek, S., Skvarca, P. (2013). Rapid retreat, acceleration and thinning of Glaciar Upsala, Southern Patagonia Icefield, initiated in 2008. Annals of Glaciology, 54(63), 131-138.

44. Sugiyama, S., M. Minowa, D. Sakakibara, P. Skvarca, T. Sawagaki, Y. Ohashi, N. Naito, and K. Chikita (2016), Thermal structure of proglacial lakes in Patagonia, J. Geophys. Res. Earth Surf., 121, 2270–2286, doi:10.1002/2016JF004084.

45. Rivera, A., Corripio, J., Bravo, C., Cisternas, S. (2012). Glaciar Jorge Montt (Chilean Patagonia) dynamics derived from photos obtained by fixed cameras and satellite image feature tracking. Annals of Glaciology, 53(60), 147-155.

46. Koppes, M., Hallet, B., Anderson, J. (2009). Synchronous acceleration of ice loss and glacier erosion, Glaciar Marinelli, Chilean Tierra del Fuego. Journal of Glaciology, 55(190), 207-220.

47. Farr, T. G., Rosen, P. A., Caro, E., Crippen, R., Duren, R., Hensley, S., Kobrick, M., Paller, M., Rodriguez, E., Roth, L., Seal, D., Shaffer, S., Shimada, J., Umland, J., Werner, M., Oskin, M., Burbank, D. & Alsdorf, D. (2007). *The Shuttle Radar Topography Mission*. Reviews of Geophysics, 45(2), RG2004. https://doi.org/10.1029/2005RG000183.

48. Dirección General de Aguas. Estimación de volúmenes de hielo en glaciares de Chile Central. Informe técnico S.I.T. N°264 (CECs para la DGA). Ministerio de Obras Públicas, Santiago, Chile, 155pp., 2011

49. Estimación de volúmenes de hielo mediante sondajes de radar en zonas norte, central y sur. Informe final S.I.T. Nº 338, Dirección General de Aguas, Ministerio de Obras Públicas, Santiago, Chile (2014).

50. Cuffey, K.M., Paterson, W.S.B. (2010). The Physics of Glaciers (4ª ed.). Butterworth-Heinemann/Elsevier.

51. Gagliardini, O., Zwinger, T., Gillet-Chaulet, F., Durand, G., de Fleurian, B., Greve, R., Malinen, M., Martín, C., Råback, P., Ruokolainen, J., Sacchettini, M., Schäfer, M., Seddik, H. & Thies, J. (2013). *Capabilities and performance of Elmer/Ice, a new-generation ice sheet model*. Geoscientific Model Development, 6, 1299–1318. https://doi.org/10.5194/gmd-6-1299-2013

768 52. Haeberli, W., and M. Hoelzle (1995), Application of inventory data for estimating characteristics of
769 and regional climate-change effects on mountain glaciers: A pilot study with the European Alps, Ann.
770 Glaciol., 21, 206–212.

771 53. Rodriguez, E., C. S. Morris, and J. E. Belz (2006), A global assess-ment of the SRTM performance,
772 Photogramm. Eng. RemoteSens., 72, 249 – 260.

773 54. Lindsay, J. B. (2016) Efficient hybrid breaching-filling sink removal methods for flow path
774 enforcement in digital elevation models. Hydrol. Process., 30: 846–857. doi: 10.1002/hyp.10648.

775 Acknowledgements (optional)

776 JB was funde by ANID/DAAD and by the Bavarian State Ministry of Science and Arts under the Elite

777 Network Bavaria (Grand reference: IDP M3OCCA) The authors are grateful for the scientific support and
778 resources provided by the Erlangen National High Performance Computing (HPC) Center (NHR@FAU)
779 of the Friedrich-Alexander-Universität Erlangen-Nürnberg (FAU). NHR funding is provided by federal and
780 Bavarian state autho rities. NHR@FAUhardwareispartiallyfundedbytheDFG—440719683. TanDEM-X
781 data were kindly provided free of charge by the German Aerospace Center (DLR) under
782 AOmabra_XTI_GLAC0264.

783 Author contributions

784 JB conceived and designed the study performed the ice thickness reconstruction and the subglacial
785 topography and future glacial lakes analysis, produce all figures and led the writing of he manuscript. JJF
786 developed the ice thickness model and designed the study. DF contributed the conceptual development of
787 the study. CS supported the modelling. MS contributed to the study concept. JLR and JU collected and
788 processed the GPR data. PI compiled the glacial lakes inventory. All author discussed the results and
789 commented on the manuscript.

790 Supplementary Information

791 **Figure S1: Cumulative ice volume against elevation for the all thickness products across the**
792 **glaciological regions of the Southern Andes. Cumulative ice volume as a function of surface**
793 **elevation for (a) The Desert Andes, (b) Central Andes, (c) The North Patagonian Andes and**
794 **(d) Southern Patagonian Andes, comparing our model (black) with Millan et al. (2022)(red),**

the consensus estimate of Farinotti et al. (2019) (Dark blue) and Frank et al. (2026) (Light blue).

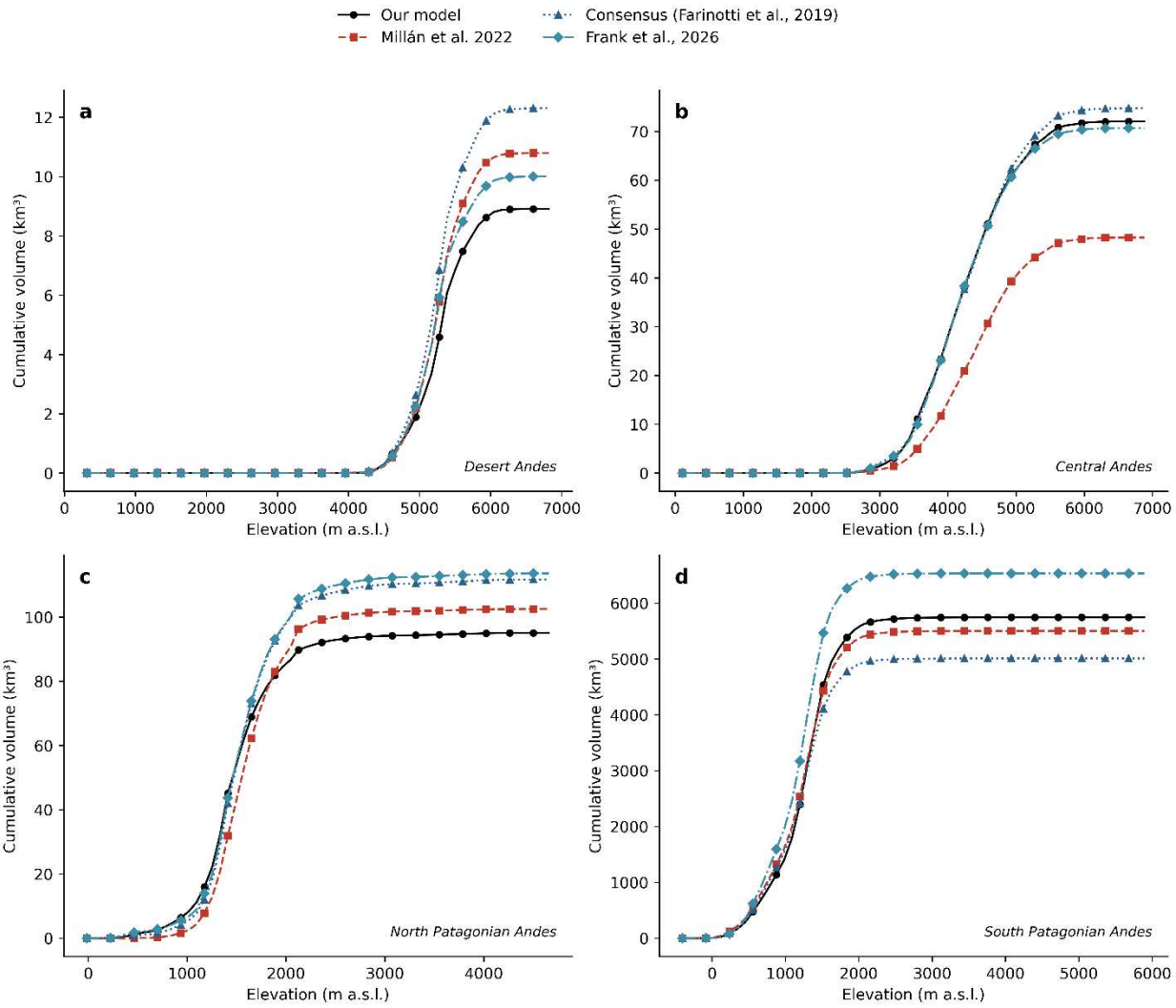
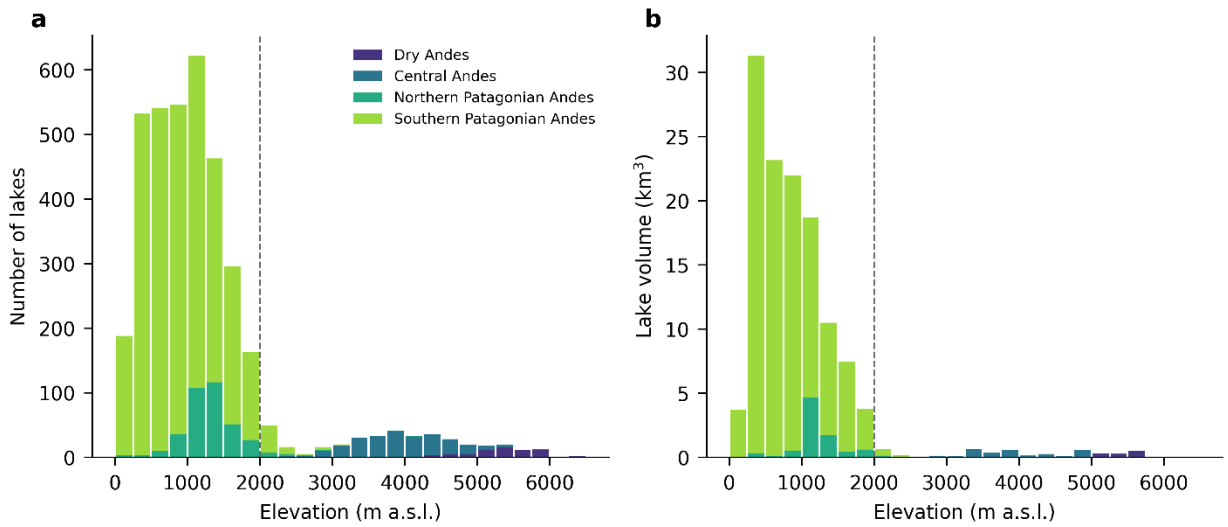
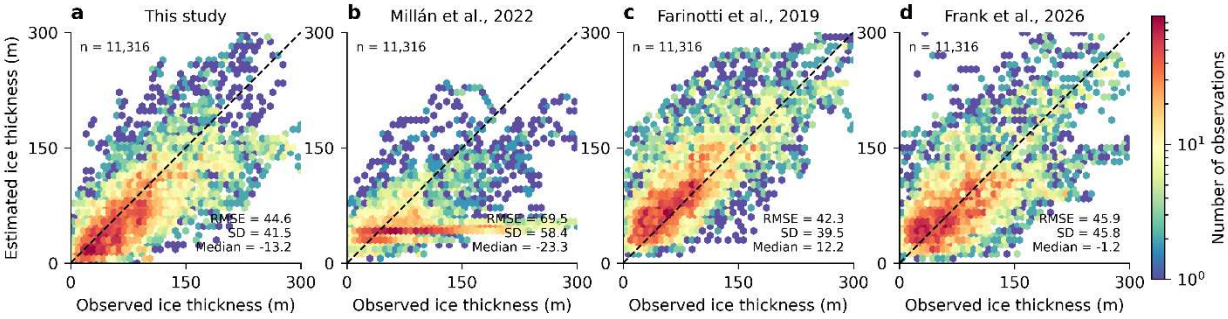


Figure S2: Elevation distribution of potential future glacial alkes across the Southern Andes (a) Number of potential glacial lakes and (b) their potential water volume, binned by elevation in 250 m.



801

802 **Figure S3: Modelled ice thickness against radar measurement in the Central Ande.**



803